Solution Structure and Conformational Changes of the *Streptomyces* Chitin-Binding Protein (CHB1)†

Dmitri I. Svergun,‡,§ Ardina Bećirević,|| Hildgund Schrempf,|| Michel H. J. Koch,‡ and Gerhard Grüber*,⊥,#

European Molecular Biology Laboratory, Hamburg Outstation, EMBL c/o DESY, Notkestrasse 85, D-22603 Hamburg, Germany, Institute of Crystallography, Russian Academy of Sciences, Leninsky pr. 59, 117333 Moscow, Russia, Abteilung Angewandte Genetik der Mikroorganismen, and Abteilung Zoophysiologie, FB Biologie/Chemie, Universität Osnabrück, D-49069 Osnabrück, Germany, and Whitney Laboratory, University of Florida, St. Augustine, Florida 32086

Received April 17, 2000; Revised Manuscript Received June 5, 2000

ABSTRACT: The shape and overall dimensions of the recently discovered *Streptomyces* α-chitin-binding protein, CHB1, were investigated by synchrotron radiation X-ray solution scattering. The radius of gyration and the maximum size of CHB1 were determined to be 1.75 ± 0.03 nm and 6.0 ± 0.2 nm, respectively. Using two independent ab initio approaches the low-resolution shape of the protein was found to consist of two domains, an elongated main globule with a length of about 4 nm and a foot-like domain of about 2 nm width. The structural and functional properties of CHB1 depend strongly on the presence of disulfide bonds; upon their reduction, the protein loses its affinity to chitin.

Streptomycetes are Gram-positive bacteria that grow as substrate hyphae and, upon depletion of nutrients, differentiate to aerial mycelia and spores. Besides their use as major producers of antibiotics, *Streptomyces* species play an ecologically important role in the degradation of chitin, using the latter as a nitrogen and carbon source (*1*, *2*). Chitin, which is the second most abundant polysaccharide in nature, consists of poly-(*N*-acetyl-D-glucosamine) chains arranged in a parallel (*β*) or an antiparallel (α) fashion (*3*, *4*) and is hydrolyzed by chitinases (*5*−*7*), which are composed of the structurally and functionally discrete catalytic and chitin-binding domain (*8*).

In addition to chitinolytic enzymes, small proteins that specifically target chitin have been found to be secreted by various *Streptomyces* strains (*9*−*12*). The molecular mass of these chitin-binding proteins are 18.7 kDa for CHB1[1] and 18.6 kDa for CHB2 as estimated from the corresponding genes of *Streptomyces olivaceoviridis* and *Streptomyces reticuli*, respectively. The two proteins consist of 201 and 200 amino acids, respectively, of which 77% are identical (*10*) and the number as well as the relative positions of tryptophan residues are conserved. Comparisons of a range of mutant proteins derived from mutated *chb1* genes have shown that two tryptophan residues are buried within the protein and one of the exposed tryptophans (Trp_{57}) plays a major role in the specific targeting of chitin by CHB1 (*11*).

Knowledge of the structure of CHB1 in conditions close to physiological is essential to understand the formation of the CHB1-chitin complex. Two independent methods (*13*, *14*) were used to retrieve the low-resolution shape of CHB1 ab initio from X-ray solution scattering data. Evidence is presented that formation of intramolecular disulfide bond(s) confers enhanced stability to the chitin-binding form of CHB1.

MATERIALS AND METHODS

Materials. Chemicals for gel electrophoresis were obtained from Serva (Heidelberg). All other chemicals were at least of analytical grade and obtained from Merck (Darmstadt), Sigma (Deisenhofen), or Serva (Heidelberg).

Purification of the Chitin-Binding Protein and Binding Tests. Streptomyces lividans pCHB10 (*9*) containing the *S. olivaceoviridis chb1* gene on a multicopy vector pWHM3 was precultivated overnight in minimal medium containing 1% glucose. Afterward, the strain was cultivated in minimal medium supplemented with 1% ground chitin from crab shells (Sigma) on a rotary shaker at 30 °C for 4 days. The culture was centrifuged (10 min, 2000×g) in order to remove crystalline chitin. The supernatant was filtered and precipitated overnight with 90% (w/v) $(NH_4)_2SO_4$. After centrifugation (40000×g, 30 min) the pellet was resuspended in 20 mM Tris/HCl (pH 7.0) and supplemented with 1.7 M $(NH_4)_2SO_4$, before loading onto a hydrophobic interaction chromatography column (Phenyl Sepharose 4 Fast Flow, Pharmacia). Fractions comprising CHB1 were pooled and precipitated with 90% (w/v) $(NH_4)_2SO_4$, centrifuged at 40000×g for 30 min, dissolved in 1 mL of 20 mM Tris/HCl, pH 7.0, and then applied to a Superdex-75 column

* To whom correspondence should be addressed. Phone: +49/(0)-541 969 3504. Fax: +49/(0)541 969 3503. E-mail: ggrueber@biologie.uni-osnabrueck.de.

† This research was supported by the Deutsche Forschungsgemeinschaft (Schr203/6-2; awarded to H.S.), by the International Association for the Promotion of Cooperation with Scientists from the Independent States of the Former Soviet Union (INTAS; to D.I S. and M.H.J.K.) Grant 96-1115, the EU Biotechnology Program Grant BIO4-CT97-2143 (to D.I.S.). G.G. was supported by the National Institutes of Health (Grant A1 22444).

‡ European Molecular Biology Laboratory.
§ Institute of Crystallography.
|| Abteilung Angewandte Genetik der Mikroorganismen.
⊥ Abteilung Zoophysiologie.
University of Florida.

[1] Abbreviations: CHB1, chitin-binding protein; DAM, dummy atom model; NMR, nuclear magnetic resonance; PAGE, polyacrylamide gel electrophoresis; SAXS, small-angle X-ray scattering; SDS, sodium dodecyl sulfate.

10.1021/bi000865p CCC: $19.00
Published on Web 08/11/2000

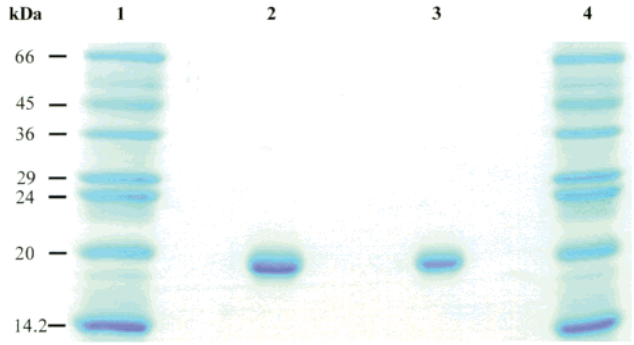

FIGURE 1: Analysis of the purified CHB1 before and after exposure to X-rays. A total of 8 μg of CHB1 were analyzed before (lane 2) and after (lane 3) exposure to X-rays under reducing conditions in a 15% polyacrylamide gel. The gel was stained with Coomassie blue. The migration positions of molecular mass standards are indicated in lanes 1 and 4.

(HR10/30, Pharmacia). The purity of CHB1 was analyzed by SDS−polyacrylamide gel electrophoresis (*15*), and the protein was identified immunologically using *anti*-CHB1 antibodies as described previously (*9*). Gels were stained with Coomassie Brilliant Blue G250. Protein concentrations were determined according to Lowry (*16*). Binding of CHB1 to the substrate α-chitin was performed according to Schnellmann et al. (*9*).

Scattering Experiments and Data Processing. The synchrotron radiation X-ray scattering data were collected using standard procedures on the X33 camera (*17*, *18*) of the EMBL on the storage ring DORIS III of the Deutsches Elektronen Synchrotron (DESY) and multiwire proportional chambers with delay line readout (*18*). The scattering curves were measured at a wavelength of $\lambda = 0.15$ nm in two ranges of momentum transfer $0.28 < s < 3.0$ nm^{-1} and $0.40 < s < 5.1$ nm^{-1} ($s = 4\pi \sin \theta/\lambda$, where 2θ is the scattering angle). The data, recorded at protein concentrations of 5 and 8 mg/mL, were normalized to the intensity of the incident beam and corrected for the detector response. The scattering of the buffer was subtracted and the difference curves were scaled for concentration using the program SAPOKO (Svergun and Koch, unpublished). Concentration effects were not detectable and the final composite scattering curve was obtained by merging the data recorded in the two *s*-ranges.

The maximum dimension D_{max} of CHB1 was estimated from the experimental data using the orthogonal expansion program ORTOGNOM (*19*). The distance distribution function $p(r)$ and the radius of gyration R_g were evaluated by the indirect Fourier transform program GNOM (*20*, *21*). The radius of gyration R_g of CHB1 was computed from the $p(r)$ function and also from the Guinier approximation (*22*, Chapter 3.3.1). The Porod volume V_p (*23*) was calculated from the processed [i.e., backtransformed from the $p(r)$] scattering curves as described in (*22*, Chapter 3.3.3). The molecular mass of the protein was estimated by comparison with forward scattering data from a reference solution of bovine serum albumin.

Shape Determination. As CHB1 is a low molecular weight protein, its X-ray scattering curve at higher angles (starting approximately from $s = 2.0$ nm^{-1}) contains significant contributions from the internal particle structure. This undesirable contribution was removed prior to the shape analysis by subtracting a constant, given by the slope of an $s^4I(s)$ vs s^4 plot, from the experimental data to ensure that the intensity would decay as s^{-4} following Porod's law (*23*) for homogeneous particles. The resulting "shape scattering" curve (i.e., scattering due to the excluded volume of the particle filled with homogeneous density) in the range of up to $s = 3.5$ nm^{-1} was used in the ab initio shape restoration of the quaternary structure. The outer portion of the curve ($s > 3.5$ nm^{-1}) that is dominated by the scattering from the internal structure was discarded in the shape analysis.

The low-resolution particle shape was restored from the experimental data using two ab initio procedures. In the method of Svergun et al. (*13*, *14*), the particle shape is

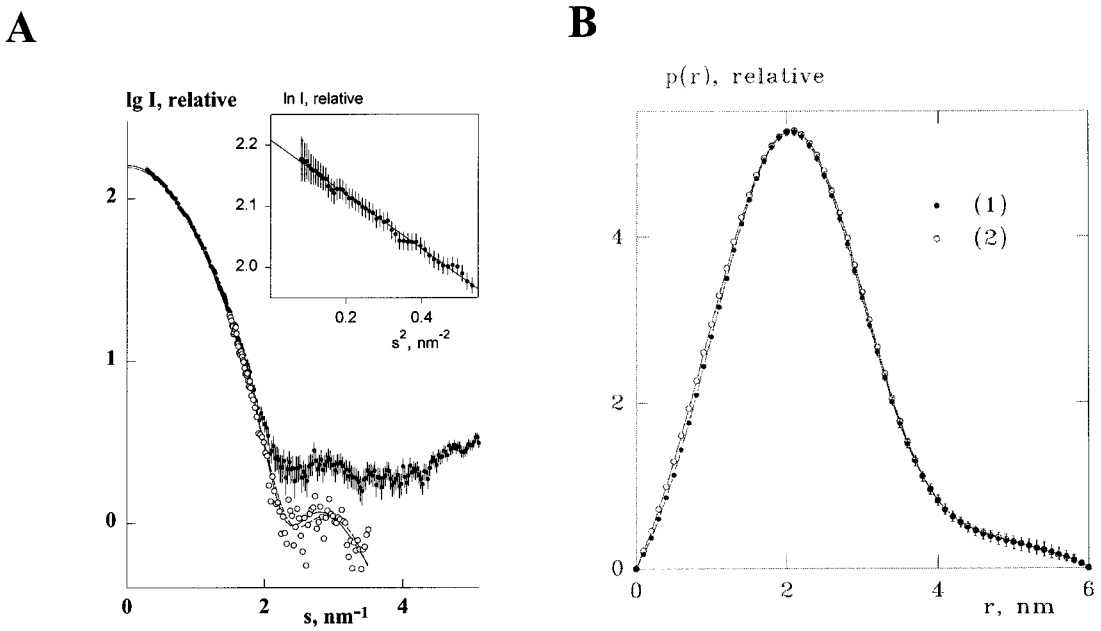

FIGURE 2: X-ray scattering and calculations. (A) X-ray scattering curves for CHB1: composite experimental curve (full circles with error bars); shape scattering curve after subtraction of a constant (open circles); scattering from the model envelope (dashed line); scattering from the dummy atom model (full line). The Guinier plot with linear fit is shown in the insert. (B) Distance distribution functions of CHB1 evaluated by the program *GNOM*. (1) Nonreduced protein corresponding to panel A; (2) reduced form of CHB1.

represented by an angular envelope function $r = F(\omega)$ where (r,ω) are spherical coordinates. The envelope is parametrized as

$$F(\omega) = \sum_{l=0}^{L} \sum_{m=-l}^{l} f_{lm} Y_{lm}(\omega) \quad (1)$$

where $Y_{lm}(\omega)$ are spherical harmonics and the multipole coefficients f_{lm} are complex numbers. The scattering intensity $I(s)$ from the envelope is evaluated as (*25*)

$$I(s) = 2\pi^2 \sum_{l=0}^{\infty} \sum_{m=-l}^{l} |A_{lm}(s)|^2 \quad (2)$$

where the partial amplitudes $A_{lm}(s)$ are calculated from the coefficients f_{lm} as described (*26*). The program *SASHA* (*13*, *24*) determines these coefficients by minimizing the discrepancy defined as

$$R^2 = \sum_{k=1}^{N} \{W(s_k)[I(s_k) - I_{exp}(s_k)]\}^2 / \sum_{k=1}^{N} [W(s_k) I_{exp}(s_k)]^2 \quad (3)$$

where N is the number of the experimental points and the weighting function is $W(s_k) = s_k^2/[\sigma(s_k)/I_{exp}(s_k)]$, $I_{exp}(s_k)$, and $\sigma(s_k)$ being the experimental intensity and its standard deviation in the k-th point, respectively. Series 1 contains $M = (L + 1)^2 - 6$ free parameters and provides a spatial resolution of approximately $\delta r = \sqrt{5\pi} R_g/[\sqrt{3}(L + 1)]$.

In the second ab initio procedure (*14*), a sphere of diameter D_{max} is filled by densely packed small spheres (dummy atoms) of radius $r_0 \ll D_{max}$. The structure of the dummy atom model (DAM) is defined by a configuration vector X assigning an index to each atom corresponding to solvent (*0*) or solute particle (*1*). The scattering intensity from the DAM is computed using eq *2* with the partial amplitudes (*14*):

$$A_{lm}(s) = i^l v_a \sqrt{2/\pi} \sum_j j_l(sr_j) Y^*_{lm}(\omega_j) \quad (4)$$

where the sum runs over the dummy atoms with $X_j = 1$ (particle atoms), r_j, and ω_j are their polar coordinates, $v_a = (4\pi r_0^3/3)/0.74$ is the displaced volume per dummy atom and $j_l(x)$ denotes the spherical Bessel function. In keeping with the low resolution of the solution scattering data, the method searches for a configuration X minimizing $f(X) = R^2 + \alpha P(X)$, where $\alpha > 0$ is a positive parameter and the penalty term $P(X)$ provides a measure of looseness and interconnectivity of the configuration. The penalty is computed by analyzing the first coordination sphere of each dummy atom. The default weight $\alpha = 0.01$ ensures a significant penalty contribution at the end of minimization so that the final solution has low resolution with respect to the packing radius r_0. Minimization is performed starting from a random configuration by fitting the processed shape scattering curve using the simulated annealing method (*27*); details of the procedure are described elsewhere (*14*, *28*).

Fluorescence Measurements. The intrinsic tryptophan fluorescence was recorded at room temperature using an SLM-AMINCO 8100 spectrofluorometer. Protein samples were excited at 280 nm, and the emission was recorded over a range of 320−370 nm. Excitation and emission band-pass were set up at 8 nm.

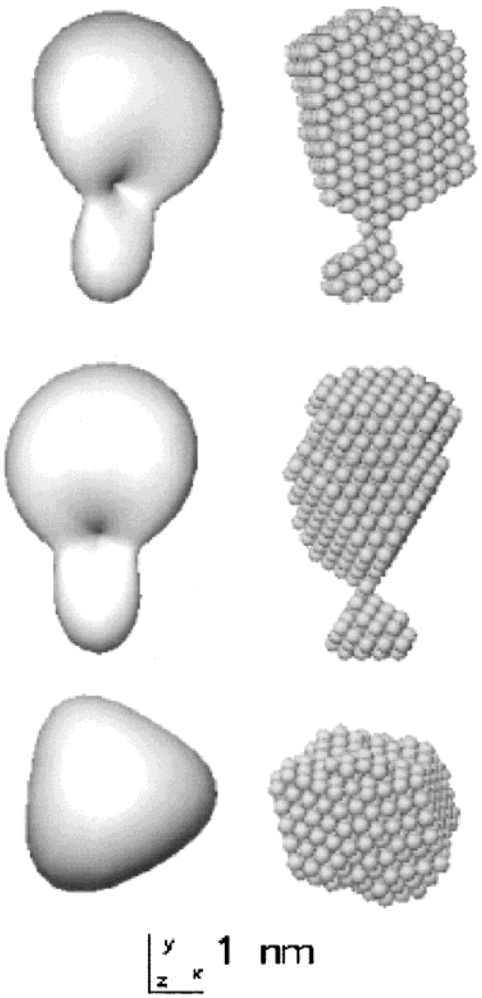

FIGURE 3: Low resolution models of CHB1. (Left panel) Envelope model, (right panel) a DAM obtained by simulated annealing. The middle and bottom rows are rotated counterclockwise by 90° around the *y*- and *x*-axes, respectively. The models were displayed on a SUN Workstation using the program *ASSA* (*43*).

RESULTS AND DISCUSSION

Overall Dimensions and the Shape of CHB1. The chitin binding protein CHB1 from the transformant *S. lividans* was highly purified (Figure 1) by sequential hydrophobic interaction chromatography and gel filtration. CHB1 was exposed to synchrotron radiation and the composite X-ray solution scattering intensity of the protein was recorded (Figure 2A). The initial portion of the scattering curve in Guinier coordinates is well approximated by a straight line (insert of Figure 2A), suggesting that the protein solution is monodisperse. The maximum dimension of CHB1 is found to be 6.0 ± 0.2 nm and as deduced both from Guinier plot and from the distance distribution function $p(r)$ its radius of gyration is 1.75 ± 0.03 nm (Figure 2B). Its molecular mass of 18 ± 1 kDa, in agreement with the value calculated from the amino acid sequence (*9*), indicates that CHB1 is monomeric in solution. Qualitative analysis of the distance distribution function suggests that CHB1 consists of a globular core yielding a principal maximum in the $p(r)$ at $0 < r < 4$ nm (Figure 2B) with a protuberance giving rise to a shoulder at $4 < r < 6$ nm.

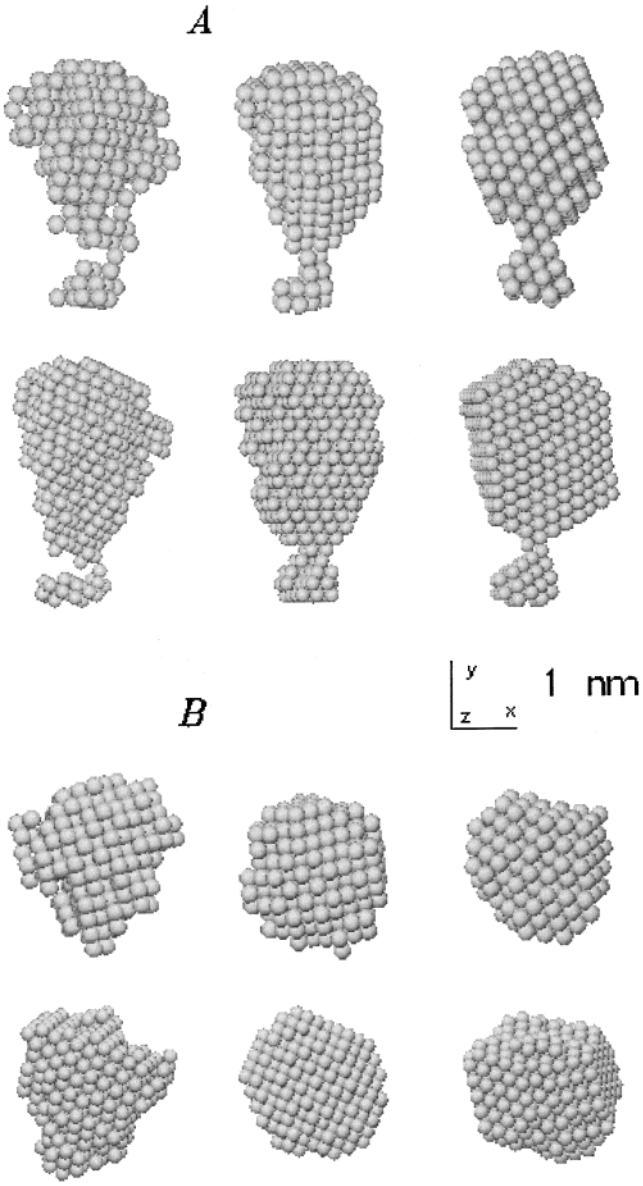

FIGURE 4: DAMs of CHB1 obtained for different values of the parameters. Top and bottom rows correspond to packing radii of 0.25 and 0.2 nm, respectively. The left, middle, and right columns correspond to penalty weights $\alpha = 0.001$, 0.005, and 0.02, respectively. In panel B, the models are rotated counterclockwise by 90° around the *x*-axis.

The "shape scattering" (Figure 2A, curve 2) obtained as described (see Materials and Methods) yields a Porod or excluded volume of the hydrated particle of 32 ± 2 nm^3, in good agreement with the molecular mass of the protein. The shape scattering curve was used to restore the low-resolution particle shape with two ab initio procedures. Shape determination using the envelope function (eq 1) is unique when the number of Shannon channels (*29*, *30*) in the data $N_s = s_{max}D_{max}/\pi$ exceeds two-thirds times the number (M) of parameters describing the envelope. The shape scattering curve of CHB1 contains $N_s = 6.6$ channels and permits to use harmonics up to $L = 3$ ($M = 10$) providing the spatial resolution $\delta r = 1.8$ nm. The restored envelope in Figure 3, left column, yields the fit to the data in Figure 2A with a residual of $R_I = 1.5 \times 10^{-2}$, a radius of gyration of $R_g = 1.73$ nm and an excluded volume $V_p = 34.0$ nm^3.

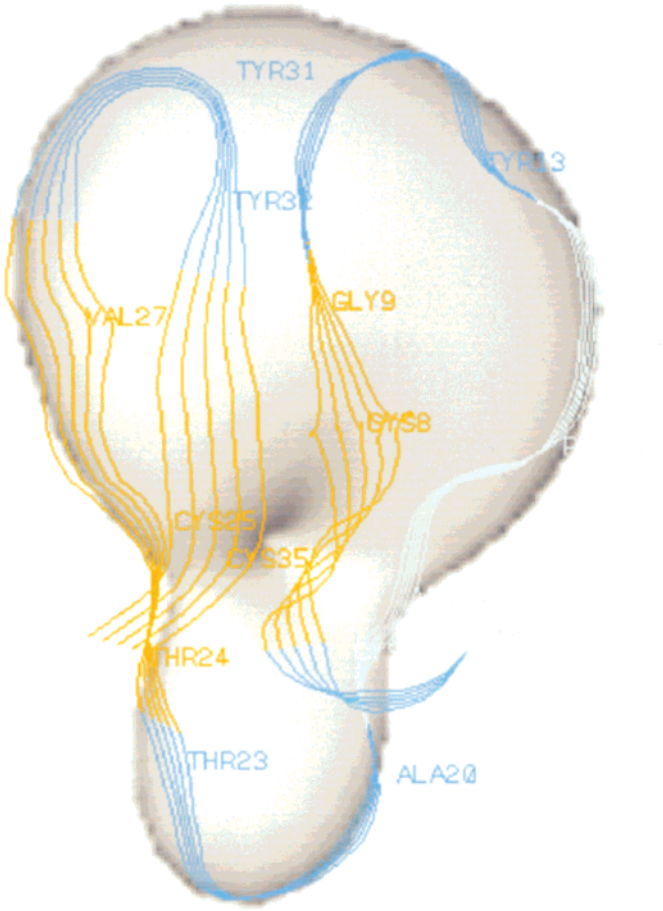

FIGURE 5: RASMOL drawing of the polypeptide backbone of CT-CBD I from *T. reesei* using NMR coordinates in the Brookhaven Protein Data Bank (*44*), entries 2cbh (*31*). β-Strands are shown in brown. The structure is superimposed on an envelope of CHB1, whose size has been reduced (1:1.8) in order to compare the structural domains of both proteins.

In the second ab initio procedure, a sphere of diameter $D_{max} = 6$ nm was filled by densely packed dummy atoms of radius $r_0 = 0.2$ nm so that the entire DAM contained a total of 2503 dummy atoms. The restored structure at the default penalty weight $\alpha = 10.02$ (Figure 3, right column) contains 697 dummy atoms, yields $R_g = 1.75$ nm and $V_p = 31.6$ nm^3, and the scattering computed from the model is indistinguishable from the processed curve (curve 4 in Figure 2A; $R_I = 2.1 \times 10^{-3}$) on the plot.

The shape determination methods yield models with an arbitrary orientation and handedness, that were appropriately rotated for comparison in Figure 3. Each of the two procedures independently yields a similarly shaped molecule consisting of an elongated main globule with a protuberance. This agreement is astonishing considering that the envelope model is described by only 10 independent parameters whereas the DAM formally has 2503 parameters. Clearly, the looseness penalty $P(X)$ drastically reduces the number of independent parameters describing the DAM in Figure 3. Note also that fitting the raw experimental data that contain significant contributions from the internal structure (curve 1 in Figure 2A) would lead to significant distortions in the final shape. This illustrates that subtraction of a constant to impose an s^{-4} decay at higher momentum transfer values is indispensable in ab initio shape determination (*14*) of a low molecular weight protein like CHB1.

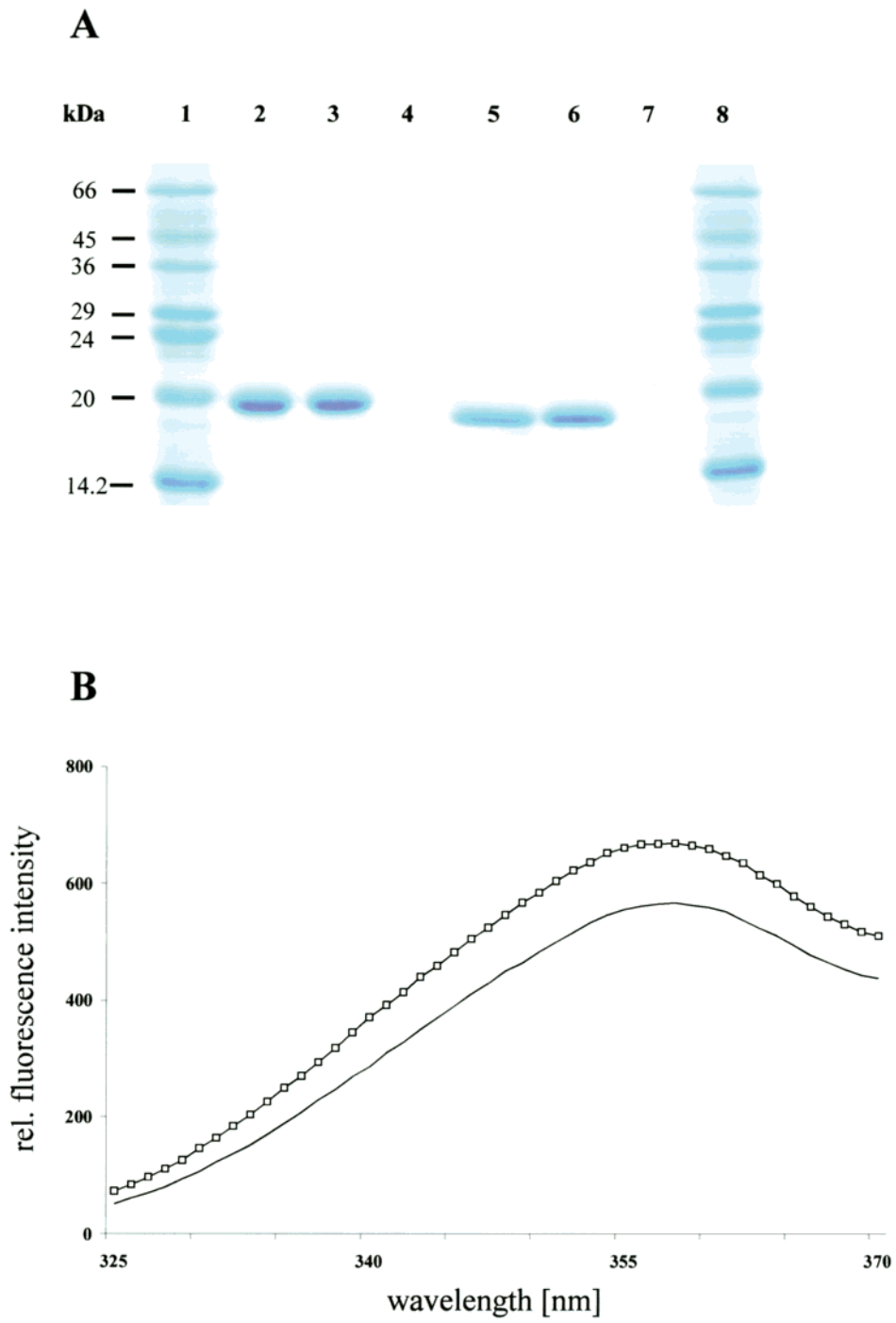

FIGURE 6: Electrophoretic and fluorescence analysis of the reduced and the oxidized form of CHB1. (A) The protein (8 μg) was incubated with (lane 2) or without (lane 5) 30 mM of DTT for 10 min in 20 mM Tris/HCl, pH 7.0, before applying to a 15% polyacrylamide gel. Lane 3, CHB1 was incubated with 5 mM $CuCl_2$ for 1 h before the addition of 30 mM DTT. Lane 6, CHB1 was supplemented with 5 mM $CuCl_2$. Lanes 4 and 7, buffer (20 mM Tris/HCl, pH 7.0). Lanes 1 and 8, molecular mass markers. (B) The fluorescence emission spectra [emission wavelength (λ_{em}) of 280 nm with emission and excitation slits at 8 nm and at λ_{ex} = 342 nm] of the CHB1 protein (53 nM) were measured at room temperature. (□) Nonreduced CHB1; (−) CHB1 after reduction by 30 mM of DTT.

To test whether the more detailed appearance of the particle shape in the simulated annealing model is justified, several independent annealing runs were performed for different DAM packing radii r_0 (0.2 and 0.25 nm) with different penalty weights (α = 0.001, 0.005, and 0.02). The six resulting models (Figure 4) yield scattering curves which are indistinguishable in the range $0 < s < 3.5$ nm^{-1}. All models display similar gross features but those obtained with a small penalty weight (α = 0.001) are clearly too detailed. In contrast, solutions corresponding to α = 0.005 and 0.02 are consistent with each other and also with the model obtained using the envelope function. Further increase of α provides yet more compact solutions but leads to detectable systematic deviations between the experimental shape scattering curve and those calculated from the final DAMs.

Altogether, CHB1 has an elongated wedgelike structure (Figure 3) with an approximately 4.0 × 3.5 nm globular domain and a 2.0 nm wide protuberance. Comparison of the low resolution structure of CHB1 with members of carbohydrate-binding proteins reveal a remarkably similar wedge-

like shape of the cellulose-binding domain (CT-CBD I) of the cellobiohydrolase I from the fungus *Trichoderma reesei*. The structure of the 36 residue CT-CBD I, deduced from magnetic resonance (NMR) spectroscopy, has dimensions of 3.0 × 1.8 × 1.0 (*31*). It is characterized by a predominantly hydrophilic face, containing the three aromatic tyrosine side chains, that were shown to be involved in cellulose binding, and other mainly hydrophobic residues. The structures of CT-CBD I and CHB1 share the same overall architecture with a main globule domain and a protuberance (Figure 5). The principal structural element in the globule domain of CT-CBD I, that includes the cellulose binding surface at one end of the structural model, is an irregular, triple-stranded antiparallel β-sheet and the protuberance is made up by the loop, consisting of the residues $Cys_{19}-Thr_{24}$ (*31*).

Disulfide Bond Formation in CHB1. Formation of disulfide bonds, a reaction that occurs rapidly in vivo, contributes to the stabilization of small proteins (*31*, *33*, *34*). CHB1 contains four cysteine residues, three within the N-terminal part ($Cys_{44,52,78}$) and the fourth at the C-terminus in position Cys_{196} (*9*). To explore the effects of disulfide bridges, the reduced and oxidized forms of CHB1 were investigated. Upon reduction by dithiothreitol (DTT), the dithiol form of the protein migrates as a band corresponding to a molecular mass of approximately 19.5 kDa (Figure 6A, lane 2). In contrast, CHB1 under nonreducing conditions migrates with an apparent molecular mass of 18.2 kDa (lane 5), close to that predicted from the amino acid sequence (*9*). The protein showed a similar behavior if disulfide formation was mediated by $CuCl_2$ (lane 6). Upon reduction by DTT (lane 3), its mobility corresponded to that of the reduced form of CHB1 (lane 2). The results indicate that CHB1 was isolated from the *S. lividans* transformant in the oxidized form. Since the mobility of the reduced CHB1 is retarded, compared to that in the oxidized form, the dithiol formation must lead either to a larger hydrodynamic volume or a lower net negative charge.

Effect of Disulfide Bond Formation on the Binding Properties of CHB1. To investigate whether disulfide formation influences the interaction of CHB1 with its substrate, a 4-fold excess (w/w) of reduced or nonreduced protein was mixed with highly purified, suspended chitin from crab shells. After centrifugation, the reduced CHB1 was found in the supernatant but did not adhere to the insoluble chitin (Figure 7, lanes 2 and 3). The major portion of the nonreduced CHB1, in contrast, bound to chitin (lane 6). The supernatant of the nonreduced form also contains unbound protein (lane 5), which is due to the excess concentration of CHB1 relative to chitin. The low ratio of unbound reduced CHB1 to chitin demonstrates that stabilized disulfide bond formation within CHB1 is essential for its targeting properties. This finding is consistent with studies of the reduced fungal cellulose-binding domain, CT-CBD I, in which DTT prevents its binding to cellulose (*35*). Like all CBDs, the CT-CBD I contains cysteine residues toward the N- and C-termini that form a disulfide bond [Figure 8 (*36*)]. Within CT-CBD I of the fungal cellobiohydrolase I, two disulfide bridges are formed by the pairs Cys_8-Cys_{25} and $Cys_{19}-Cys_{35}$ [Figure 5 (*31*)].

Spectroscopic Investigations. CHB1 contains five tryptophan residues, four at the N-terminus ($Trp_{57,99,114,134}$), and

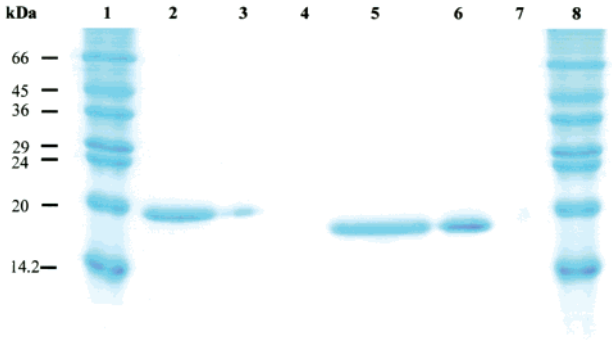

FIGURE 7: Effect of disulfide bond formation on the chitin-binding properties of CHB1. Before incubation with chitin (16 h) the protein was supplemented with (lanes 2 and 3) or without (lanes 5 and 6) 30 mM of DTT. After two washes with buffer A (136 mM NaCl, 2.6 mM KCl, 1.4 mM KH_2PO_4, and 8.1 mM Na_2HPO_4, pH 7.1) and with buffer A plus 1 M NaCl, both samples were centrifuged at 10000×g for 5 min in order to separate unbound CHB1 from the chitin-protein complex. Identical amounts of dissolved pellet (lanes 3 and 6) and supernatant (lanes 2 and 5) were applied onto a 15% polyacrylamide gel. Lanes 1 and 8, standard proteins.

FIGURE 8: N- and C-terminal amino acid sequence alignment of CHB1 (*9*) and CT-CBD I (*31*). Identical amino acids are indicated by black-shaded frames and similar amino acids with light-shaded frames, respectively. Conservative Cys-residues are marked by an asterisk. Dots indicate gaps for alignment of both termini.

the other at position Trp_{184} (*9*). To obtain additional information on the structural properties of the reduced and nonreduced CHB1, the fluorescence emission of both states was monitored using the intrinsic tryptophan fluorescence. The reduction of CHB1 (Figure 6B) causes the quantum yield to decrease, suggesting that at least one tryptophan residue interacts with side-chains which efficiently quench its fluorescence (*37*). Previous studies (*11*) had revealed that a replacement of each of the five tryptophan residues by leucine (Leu) led to formation of mutant proteins targeting chitin to varyingly reduced degrees. The Trp_{57} residue of CHB1 was shown to be directly involved in the interaction with chitin. An interaction of the N-terminal region including the residue Trp_{57} with chitin is also in line with the observation that conserved aromatic residues such as tryptophan and tyrosin (see Figure 5) within CBDs are involved in cellulose binding as shown by mutagenesis studies, NMR spectroscopy, and X-ray crystallography (*31*, *38*−*42*).

Effect of Reduction on the Overall Structure of CHB1 Studied by SAXS. The conformational changes were investigated further by X-ray scattering in order to determine whether they were accompanied by changes of the quaternary structure of CHB1. The radius of gyration for the nonreduced and the reduced complex of CHB1 was found to coincide within experimental error. The scattering curves (not shown) and the corresponding distance distribution functions (Figure 2B) nearly coincide indicating that the quaternary structure of the oxidized form does not diverge from that of the reduced CHB1. This finding implicates that the altered property of the reduced CHB1, as compared to the oxidized form, is mainly caused by changes of the secondary structure, as a result of disulfide formation and/or interaction of tryptophan residue(s) with side chains. Moreover, the retarded

mobility of the reduced CHB1 must rather be caused by a lower net negative charge than by a larger hydrodynamic volume.

The quaternary structures obtained using two ab initio shape restoration procedures show independently that CHB1 is organized as two well-defined domains, with a major domain approximately 4 nm long and a protuberance with a diameter of approximately 2 nm. Binding studies suggest that only CHB1 stabilized by disulfide bond(s) forms a stable complex with chitin. The change in fluorescence after reduction of the protein reflects conformational changes due to abolition of disulfide bond(s). It remains to be determined whether the region that targets the polysaccharide in CHB1 corresponds to one end of the globular domain, as described for CT-CBD I.

REFERENCES

1. Kutzner, H. J. (1981) in *The Prokaryotes: A Handbook on Habitats, Isolation and Identification of Bacteria* (Starr, M. P., Stolp, H., Trüper, H. G., Balows, A., and Schlegel, H., Eds.) Springer-Verlag, Berlin.
2. Williams, S. T., and Robinson, C. S. (1981) *J. Gen. Microbiol. 127*, 55−63.
3. Ramakrishnan, C., and Prasdad, N. (1972) *Biochim. Biophys. Acta 261*, 123−135.
4. Muzzarelli, R. A. A. (1977) *Chitin*, Pergamon Press, Oxford.
5. Beyer, M., and Diekmann, H. (1985) *Appl. Microbiol. Biotechnol. 23*, 140−146.
6. Robbins, P. W., Albright, C., and Benfield, B. (1988) *J. Biol. Chem. 263*, 443−447.
7. Romaguera, A., Menge, U., Breves, R., and Diekmann, H. (1992) *J. Bacteriol. 174*, 3450−3454.
8. Blaak, H., Schnellmann, J., Walter, S., Henrissat, B., and Schrempf, H. (1993) *Eur. J. Biochem. 214*, 659−669.
9. Schnellmann, J., Zeltins, A., Blaak, H., and Schrempf, H. (1994) *Mol. Microbiol. 13*, 807−819.
10. Kolbe, S., Fischer, A., Bećirević, A., Hinz, P., and Schrempf, H. (1998) *Microbiology 144*, 1291−1297.
11. Zeltins, A., and Schrempf, H. (1997) *Eur. J. Biochem. 246*, 557−564.
12. Schrempf, H., Kolbe, S., Bećirević, A., and Zeltins, A. (1999) in *Recent Advances in Carbohydrate Bioengineering* (Gilbert, H. J., Davies, G. J., Henrissat, B., and Svensson, B., Eds.) pp 227−231, The Royal Society of Chemistry.
13. Svergun, D. I., Volkov, V. V., Kozin, M. B., and Stuhrmann, H. B. (1996) *Acta Crystallogr., Sect. A 52*, 419−426.
14. Svergun, D. I. (1999) *Biophys. J. 76*, 2879−2886.
15. Laemmli, U. K. (1970) *Nature 227*, 680−685.
16. Lowry, O. H., Rosebrough, N. J., Farr, A. L., and Randall, R. J. (1951) *J. Biol. Chem. 193*, 265−275.
17. Koch, M. H. J., and Bordas, J. (1983) *Nucl. Instrum. Methods 208*, 461−469.
18. Boulin, C. J., Kempf, R., Gabriel, A., and Koch, M. H. J. (1988) *Nucl. Instrum. Methods A 269*, 312−320.
19. Svergun, D. I. (1993) *J. Appl. Crystallogr. 26*, 258−267.
20. Svergun, D. I., Semenyuk, A. V., and Feigin, L. A. (1988) *Acta Crystallogr., Sect. A 44*, 244−250.
21. Svergun, D. I. (1992) *J. Appl. Crystallogr. 25*, 495−503.
22. Feigin, L. A., and Svergun, D. I. (1987) *Structure analysis by small-angle X-ray and neutron scattering*, Plenum Press, New York.
23. Porod, G. (1982) *General theory*. in *Small-angle X-ray scattering* (Glatter, O., and Kratky, O., Eds.) pp 17−51, Academic Press, London.
24. Svergun, D. I., Volkov, V. V., Kozin, M. B., Stuhrmann, H. B., Barberato, C., and Koch, M. H. J. (1997) *J. Appl. Crystallogr. 30*, 798−802.
25. Stuhrmann, H. B. (1970) *Zeitschr. Physik. Chem. Neue Folge 72*, 177−198.
26. Svergun, D. I., and Stuhrmann, H. B. (1991) *Acta Crystallogr., Sect. A 47*, 736−744.
27. Kirkpatrick, S., Gelatt, C. D., Jr., and Vecci, M. P. (1983) *Science 220*, 671−680.
28. Svergun, D. I., Malfois, M., Koch, M. H. J., Wigneshweraraj, S. R., and Buck, M. (2000) *J. Biol. Chem. 275*, 4210−4214.
29. Shannon, C. E., and Weaver, W. (1949) *The mathematical theory of communication*, University of Illinois Press, Urbana.
30. Moore, P. B. (1980) *J. Appl. Crystallogr. 13*, 168−175.
31. Kraulis, P. J., Clore, G. M., Nilges, M., Jones, T. A., Pettersson, G., Knowles, J., and Gronenborn, A. M. (1989) *Biochemistry 28*, 7241−7257.
32. Xu, G. Y., Ong, E., Gilkes, N. R., Kilburn, D. G., Muhandiram, D. R., Harris-Brandts, M., Carver, J. P., Kay, L. E., and Harvey, T. S. (1995) *Biochemistry 34*, 6993−7009.
33. Doig, A. J., and Williams, D. H. (1991) *J. Mol. Biol. 217*, 389−398.
34. Besette, P. H., Åslund, F., Beckwith, J., and Georgiou, G. (1999) *Proc. Natl. Acad. Sci U.S.A. 96*, 13703−13708.
35. Johansson, G., Ståhlberg, J., Lindeberg, G., Engström, Å., and Pettersson, G. (1989) *FEBS Lett. 243*, 389−393.
36. Gilkes, N. R., Henrissat, B., Kilburn, D. G., Miller, Jr., R. C., and Warren, R. A. J. (1991) *Microbiol. Rev. 55*, 303−315.
37. Lakowicz, J. R. (1983) *Principles of Fluorescence Spectroscopy*, Plenum Press, New York.
38. Din, N., Forsythe, I. J., Burtnick, L. D., Gilkes, N. R., Miller, R. C., Jr., Warren, R. A. J., and Kilburn, D. G. (1994) *Mol. Microbiol. 11*, 747−755.
39. Poole, D. M., Hazlewood, G. P., Huskisson, N. S., Virden, R., and Gilbert, H. J. (1993) *FEMS Microbiol Lett. 106*, 77−84.
40. Ponyi, T., Szabó, L., Nagy, T., Orosz, L., Simpson, P. J., Williamson, M. P., and Gilbert, H. J. (2000) *Biochemistry 39*, 985−991.
41. Boraston, A. B., McLean, B. W., Kormos, J. M., Alam, M., Gilkes, N. R., Haynes, C. A., Tomme, P., Kilburn, D. G., and Warren, R. A. J. (1999) in *Recent Advances in Carbohydrate Bioengineering* (Gilbert, H. J., Davies, G. J., Henrissat, B., and Svensson, B., Eds.) pp 202−211, The Royal Society of Chemistry, Cambridge.
42. Tormo, J., Lamed, R., Chirino, A. J., Morag, E., Bayer, E. A., Shoham, Y., and Steitz, T. A. (1996) *EMBO J. 15*, 5739−5751.
43. Kozin, M. B., Volkov, V. V., and Svergun, D. I. (1997) *J. Appl. Crystallogr. 30*, 811−815.
44. Bernstein, F. C., Koetzle, T. F., Williams, G. J. B., Meyer, E. G., Jr., Brice, M. D., Rodgers, J. R., Kennard, O., Shimanouchi, T., and Tasumi, M. (1977) *J. Mol. Biol. 112*, 535−542.

BI000865P